A fluorescent tagging approach in *Drosophila* reveals late endosomal trafficking of Notch and Sanpodo

Lydie Couturier,[1,2] Mateusz Trylinski,[1,2,3] Khallil Mazouni,[1,2] Léa Darnet,[1,2] and François Schweisguth[1,2]

[1]Developmental and Stem Cell Biology Department, Institut Pasteur, 75015 Paris, France
[2]Centre National de la Recherche Scientifique, URA2578, 75015 Paris, France
[3]Master Biosciences, École Normale Supérieure de Lyon, 75015 Paris, France

Signaling and endocytosis are highly integrated processes that regulate cell fate. In the *Drosophila melanogaster* sensory bristle lineages, Numb inhibits the recycling of Notch and its trafficking partner Sanpodo (Spdo) to regulate cell fate after asymmetric cell division. In this paper, we have used a dual GFP/Cherry tagging approach to study the distribution and endosomal sorting of Notch and Spdo in living pupae. The specific properties of GFP, i.e., quenching at low pH, and Cherry, i.e., slow maturation time, revealed distinct pools of Notch and Spdo: cargoes exhibiting high GFP/low Cherry fluorescence intensities localized mostly at the plasma membrane and early/sorting endosomes, whereas low GFP/high Cherry cargoes accumulated in late acidic endosomes. These properties were used to show that Spdo is sorted toward late endosomes in a Numb-dependent manner. This dual-tagging approach should be generally applicable to study the trafficking dynamics of membrane proteins in living cells and tissues.

Introduction

Cell–cell communication is essential for the development and homeostasis of multicellular organisms. Signaling by cell surface receptors and endocytosis are highly integrated processes (Seto et al., 2002; Le Borgne et al., 2005; Polo and Di Fiore, 2006; Collinet et al., 2010). The interplay between membrane trafficking and cell–cell signaling has been well studied in the context of sensory organs in *Drosophila melanogaster* (Kandachar and Roegiers, 2012). The sensory bristles of adult flies are produced during metamorphosis from sensory organ precursor cells (SOPs; Hartenstein and Posakony, 1989). SOPs divide via a stereotyped lineage to generate the four different sensory cells (Gho et al., 1999). In a first division, SOPs divide asymmetrically along the body axis to generate an anterior pIIb and a posterior pIIa cell (Gho and Schweisguth, 1998). Notch regulates the pIIa/pIIb cell fate decision (Hartenstein and Posakony, 1990). High Notch activity specifies the pIIa fate. Notch activation in pIIa depends on Delta and Serrate, the two ligands of Notch in *Drosophila* (Zeng et al., 1998). Activation of Notch in pIIa, and not pIIb, is in part achieved via the unequal segregation of the E3 ubiquitin ligase Neuralized (Neur), a positive regulator of Delta, into pIIb (Lai et al., 2001; Pavlopoulos et al., 2001; Le Borgne and Schweisguth, 2003). Conversely, low Notch activity specifies the pIIb fate. Inhibition of Notch in pIIb requires the activity of Numb (Uemura et al., 1989). Numb is a conserved multifunctional protein that regulates endocytosis in various model systems (Santolini et al., 2000; Berdnik et al., 2002; Smith et al., 2004; Nishimura and Kaibuchi, 2007; Nilsson et al., 2008; Sato et al., 2011). In dividing SOPs, Numb localizes at the anterior cortex and is inherited by the anterior pIIb cell (Rhyu et al., 1994). Numb has been suggested to regulate the endocytosis of Notch (Santolini et al., 2000; Berdnik et al., 2002; Smith et al., 2004; Couturier et al., 2012; Song and Lu, 2012; Krieger et al., 2013) and/or Sanpodo (Spdo), a positive regulator of Notch (O'Connor-Giles and Skeath, 2003; Hutterer and Knoblich, 2005; Tong et al., 2010; Couturier et al.,

Correspondence to François Schweisguth: fschweis@pasteur.fr

Abbreviations used in this paper: APF, after puparium formation; BAC, bacterial artificial chromosome; Cad, cadherin; FRET, Forster resonance energy transfer; IQR, interquartile range; *krz, kurtz; lgd, lethal(2) giant discs*; Neur, Neuralized; NICD, Notch intracellular domain; NiCherry, Notch intracellular Cherry; NiGFP, Notch intracellular GFP; Rbcn-3A, Rabconnectin-3A; sfGFP, superfolder GFP; SOP, sensory organ precursor cell; Spdo, Sanpodo.

The Rockefeller University Press $30.00
J. Cell Biol. Vol. 207 No. 3 351–363
www.jcb.org/cgi/doi/10.1083/jcb.201407071

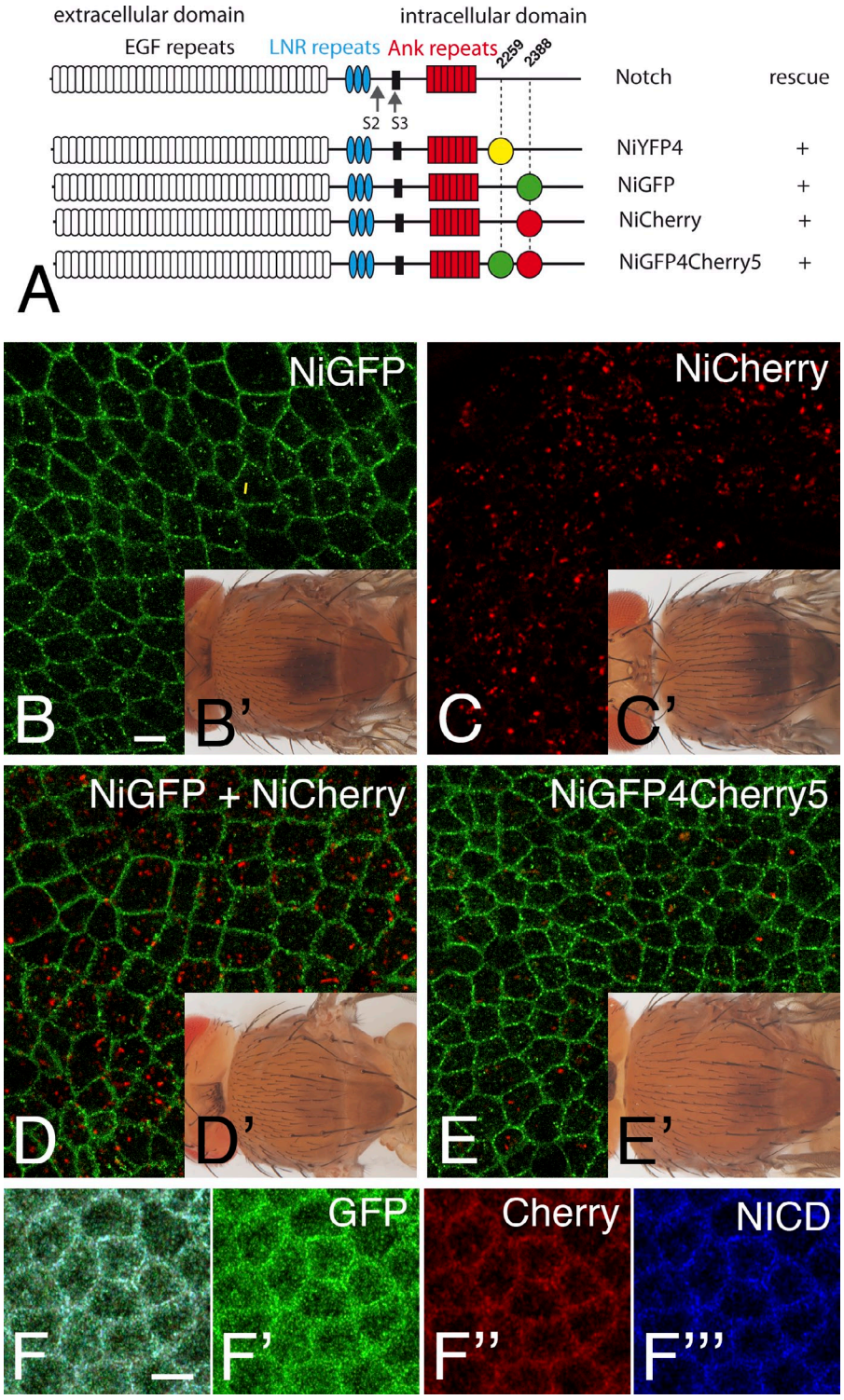

Figure 1. **GFP and Cherry highlighted distinct pools of Notch.** (A) Structure of Notch showing the EGF-like repeats, Lin-12 Notch repeats (LNR), and ankyrin (Ank) repeats and the transmembrane segment (black). NiYFP4 and NiGFP were described previously (Couturier et al., 2012). Cherry was inserted at position 2,388 in NiCherry and NiGF4Cherry5 (same position as in NiGFP). GFP was inserted at position 2,259 in NiGFP4Cherry5 (same position as in NYFP4). All BAC-encoded tagged receptors rescued the null N^{55e11} mutation. (B–E′) GFP (green in B, D, and E) and Cherry (C, D, and E) fluorescence signals in the notum of living NiGFP (B), NiCherry (C), NiGFP/NiCherry (D), and NiGFP4Cherry5 (E) 16–17 h after puparium formation (APF) in male pupae hemizygous for N^{55e11} (see Table S1 for detailed genotypes of this and all other figures). Rescued NiGFP (B′), NiCherry (C′), NiGFP/NiCherry (D′), and NiGFP4Cherry5 (E′) N^{55e11} mutant flies are shown in insets. (F–F‴) GFP (anti-GFP, green) and Cherry (anti-DsRed, red) epitopes of NiGFP4Cherry5 colocalized with intracellular Notch (NICD) epitopes at the apical cortex in the notum of NiGFP4Cherry5 pupae mutant for N^{55e11}. Bars, 5 µm.

2012; Upadhyay et al., 2013), to direct Notch toward degradation (McGill et al., 2009) and/or to inhibit its recycling (Smith et al., 2004; Nilsson et al., 2008; Cotton et al., 2013; Couturier et al., 2013). Whereas recent studies have indicated that Numb delays the recycling of Spdo–Notch complexes in pIIb (Cotton et al., 2013; Couturier et al., 2013), whether internalized Spdo and Notch are sorted toward late endosomal degradation remains to be addressed.

Here, we use a novel dual GFP/Cherry tagging approach to study the trafficking of Notch and Spdo in living flies. We find that both the slow maturation time of Cherry (relative to GFP) and the pH sensitivity of GFP (relative to Cherry) could be used to monitor the path followed by Notch and Spdo from the plasma membrane to late acidic endosomes. Using dual-tagged sensors, we show that internalized Spdo is sorted toward late endosomes in the Numb-inheriting SOP daughter

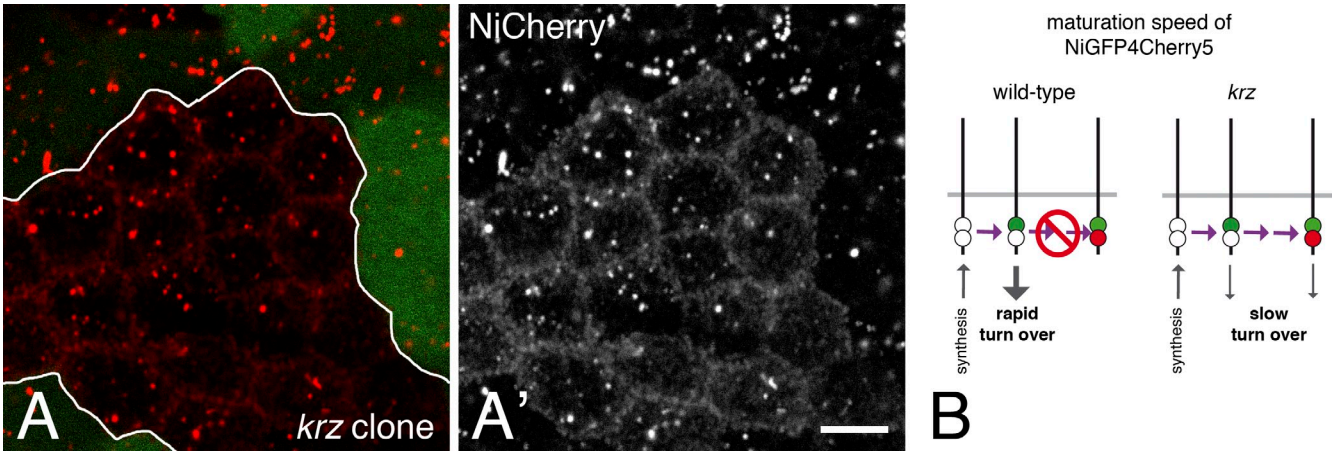

Figure 2. **Maturation of Cherry-tagged Notch.** (A and A′) Cherry fluorescence of NiCherry (red) was detected at the apical plasma membrane in *krz* mutant cells (marked by the loss of the GFP marker; clone border indicated in white) but not in wild-type cells. This indicated that slowing down the turnover of Notch at the cell surface by removing the activity of *krz* allowed for the maturation of Cherry. Bar, 5 µm. (B) Diagram illustrating the time-dependent maturation of NiGFP4Cherry5. Initially, dark NiGFP4Cherry5 (white spots) is synthesized. Because GFP is maturing faster than Cherry, bright NiGFP4Cherry5 mostly include GFP-positive (green spot) molecules when turnover is rapid (wild-type cells, left), whereas some GFP/Cherry-positive molecules (green and red spots) could be detected when turnover is slow (*krz* mutant cells, right). The horizontal purple arrow indicates time.

cell. Moreover, we observe that the endosomal pool of Notch is symmetrically distributed at cytokinesis between SOP daughter cells. Thus, our study indicates that dual-tagged sensors can be used to study the trafficking dynamics of membrane proteins in living cells.

Results

GFP and Cherry revealed distinct pools of Notch

Live imaging of GFP-tagged Notch, Numb, and Spdo suggested that these proteins might colocalize at apical endosomes in pIIb (Couturier et al., 2013). To study the colocalization of Notch with Spdo and Numb in living flies, we generated a bacterial artificial chromosome (BAC) transgene encoding a Notch-Cherry receptor, Notch intracellular Cherry (NiCherry; Fig. 1 A, Cherry was inserted at the same position as GFP in Notch intracellular GFP [NiGFP]). This transgene fully rescued a *Notch*-null mutation, indicating that NiCherry, like NiGFP, was fully functional (Fig. 1, B′ and C′; Couturier et al., 2012). Unlike NiGFP, however, NiCherry was not detected at cell–cell contacts in the dorsal thorax epithelium, or notum, of living pupae (Fig. 1, B and C), and the Cherry fluorescence of NiCherry was detected at intracellular dots. This difference in NiGFP and NiCherry fluorescence was clearly seen in flies carrying both transgenes (Fig. 1, D and D′). To test whether this resulted from differences in protein localization and/or fluorescence properties, we generated NiGFP4Cherry5 (Fig. 1 A), a receptor tagged with GFP at position 4 (insertion at this position did not affect the activity of Notch in NYFP4; Couturier et al., 2012) and Cherry at position 5 (as in NiCherry). Rescue assay showed that NiGFP4Cherry5 was fully functional (Fig. 1 E′). The GFP signal of NiGFP4Cherry5 was detected at cell–cell contact regions as well as in small apical dots, whereas the Cherry signal revealed a distinct pool of larger intracellular dots. In contrast, the GFP, Cherry, and Notch intracellular domain (NICD) epitopes of NiGFP4Cherry5 colocalized at apical cell–cell contacts in fixed tissue (Fig. 1 F–F‴). Since Western blot analysis revealed no unexpected proteolytic products (Fig. S1), we conclude that the different distribution patterns of NiGFP4Cherry5 seen with GFP and Cherry were caused by differences in fluorescence properties and not in protein distribution. Thus, GFP and Cherry appeared to reveal distinct pools of NiGFP4Cherry5 within living cells. Also, Cherry could not be used to study the colocalization of Notch with GFP-tagged Spdo and Numb in living cells.

Slow maturation time of Cherry relative to the turnover of Notch

One possible difference between GFP and Cherry is maturation speed, which depends on the kinetics of both protein folding and chromophore maturation (Verkhusha et al., 2001; Shaner et al., 2005; Merzlyak et al., 2007; Subach et al., 2009; Iizuka et al., 2011; Macdonald et al., 2012; Hebisch et al., 2013). Although measured maturation speed varied greatly depending on experimental approaches, it is usually considered to be in the 5–20- and 40–80-min range for GFP and Cherry, respectively, at 37°C (Verkhusha et al., 2001; Shaner et al., 2005; Merzlyak et al., 2007; Subach et al., 2009; Iizuka et al., 2011; Macdonald et al., 2012; Hebisch et al., 2013). Of note, longer maturation times were measured at 20°C (Verkhusha et al., 2001; Shaner et al., 2005; Merzlyak et al., 2007; Subach et al., 2009; Iizuka et al., 2011; Macdonald et al., 2012; Hebisch et al., 2013), close to the temperature at which flies are usually kept (25°C). This difference in maturation time has previously been used to design a fluorescent timer that reports on the stability of cytoplasmic proteins (Khmelinskii et al., 2012). Thus, the very weak Cherry fluorescence of NiCherry and NiGFP4Cherry5 at the plasma membrane relative to GFP of NiGFP or NiGFP4Cherry5 might result from the slower maturation of Cherry. Accordingly, Notch at the plasma membrane would mostly correspond to recently synthesized molecules. To test this interpretation, we studied the fluorescence of NiGFP4Cherry5 in

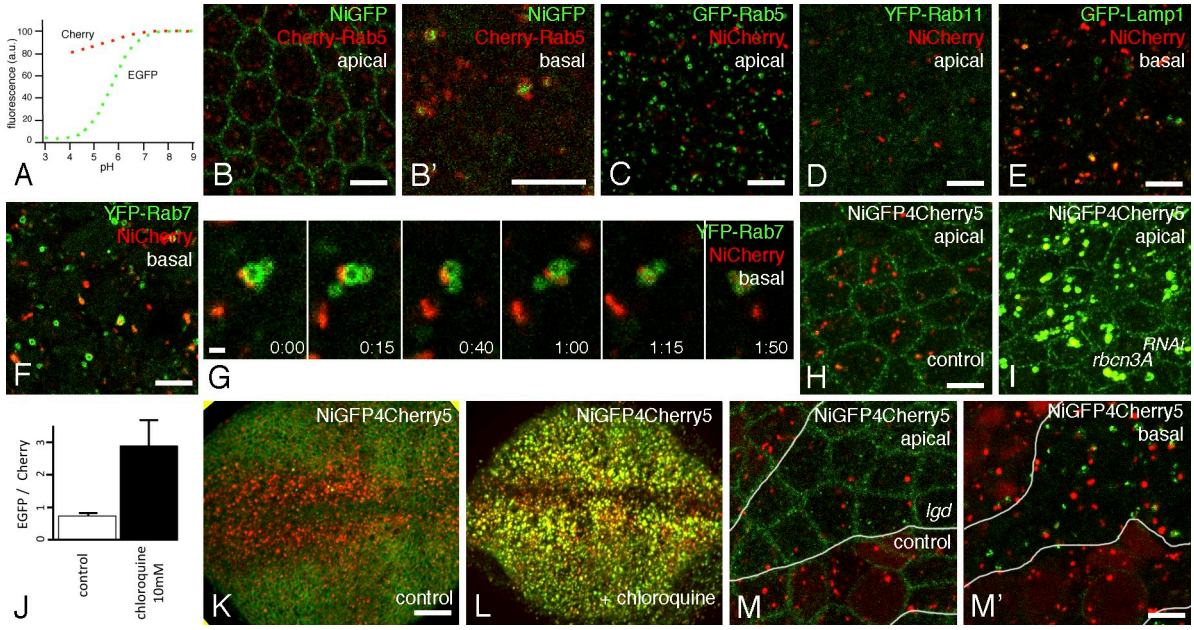

Figure 3. **pH-dependent fluorescence of tagged Notch in endosomes.** (A) pH-dependent emission profiles of GFP and Cherry (adapted from Doherty et al., 2010). a.u., arbitrary unit. (B and B′) intracellular NiGFP (GFP) remained associated with Cherry-Rab5 endosomes in living pupae. See also Video 1. (C–G) NiCherry (Cherry) did not colocalize with GFP-Rab5 (GFP in C; see also Video 3) nor YFP-Rab11 (YFP in D) but partly overlapped with GFP-Lamp1 (GFP in E) and YFP-Rab7 (YFP in F and G; see also Video 4). Snapshots of a video showing the tethering and fusion of NiCherry-positive endosomes with YFP-Rab7 endosomes (G; *t* is in minutes and seconds). (H and I) Live imaging of NiGFP4Cherry5 in living pupae in control (H) and *Rbcn-3A*^{RNAi} pupae. The silencing of *Rbcn-3A* led to the detection of GFP (green) and Cherry (red) fluorescence in enlarged Notch-containing endosomes in living notum cells. (J–L) Imaging of NiGFP4Cherry5 of living third instar larvae showing the pouch of wing imaginal discs in control (K) and chloroquine-fed (L) N^{55e11} rescued larvae. In control larvae, GFP showed the apical cortex of wing pouch cells and Cherry revealed intracellular dots, particularly along the anterior wing margin, a region of high Delta-Notch signaling. Upon chloroquine treatment, the GFP and Cherry signals of NiGFP4Cherry5 colocalized in dots (L), and the GFP/Cherry signal intensity ratio was significantly increased (J). Error bars represent the standard error of the mean ($n = 5$). (M and M′) Apical distribution of NiGFP4Cherry5 (GFP [green] and Cherry [red]) was largely unaffected by the loss of *lgd* activity (M; mutant cells were marked by the loss of a nuclear RFP marker) in living genetically mosaic pupae. In contrast, enlarged high GFP and low Cherry endosomes were specifically detected basally in *lgd* mutant cells (M′). The number and size of the high Cherry endosomes was not detectably changed upon the loss of *lgd* activity (M′; this observation was confirmed using GFP as a clone marker; not depicted). The white lines indicate the borders of the mutant clone. Bars: (B–F, H, and M′) 5 µm; (G) 1 µm; (K) 25 µm.

cells that are mutant for the nonvisual β-arrestin gene known as *kurtz* (*krz*) in flies. The activity of *krz* is required to down-regulate Notch: in *krz* mutant cells, Notch accumulated at the cell surface (Mukherjee et al., 2005). Here, we found that the Cherry fluorescence of NiCherry was clearly detectable at the cortex of *krz* mutant cells (Fig. 2, A and A′). Thus, slowing down the turnover of Notch allowed the detection of the Cherry fluorescence of NiCherry at the plasma membrane. We therefore suggest that the Cherry fluorescence of NiGFP4Cherry5 was not detectable at the plasma membrane as a result of the rapid turnover of Notch and the slow maturation of Cherry (Fig. 2 B).

Detecting Notch in acidic endosomes via the quenching of GFP at low pH

A second difference between GFP and Cherry is pH sensitivity. Indeed, the reported pKa (acid dissociation constant) of EGFP and Cherry are 6.0 and <4.5, respectively (Fig. 3 A; Shaner et al., 2005; Doherty et al., 2010). Indeed, GFP fluorescence reversibly responds within seconds to pH changes (Kneen et al., 1998; Taylor et al., 2011). Clearly, this property has in vivo relevance because early endosomes, late endosomes, and lysosomes have a pH in the 6.1–6.8, 4.8–6.0, and <4.5 range, respectively (Yamashiro and Maxfield, 1987; Huotari and Helenius, 2011), and this difference has been used to design reporters for acidic autophagic compartments (Kimura et al., 2007). The quenching of GFP at low pH therefore suggested that the GFP-negative, Cherry-positive intracellular dots might correspond to acidic intracellular vesicles.

To test this hypothesis, we studied the endosomal localization of NiGFP and NiCherry in living cells. Live imaging of NiGFP showed that the apical GFP-positive dots remained associated with early/sorting endosomes marked by Cherry-Rab5 and Cherry-Rab4 (Fig. 3, B and B′; Video 1; and Video 2). This indicated that the GFP fluorescence of NiGFP revealed a pool of Notch localizing at early/sorting endosomes. In contrast, the Cherry fluorescent dots of NiCherry did not colocalize with GFP-Rab5 endosomes (Fig. 3 C and Video 3; note that GFP-Rab5 largely colocalized with Cherry-Rab5 with the exception of strong Cherry-positive, GFP-negative dots that might correspond to acidic autophagosomes; Kimura et al., 2007). Also, NiCherry did not colocalize with YFP-Rab11 (Fig. 3 D). However, many Cherry-positive NiCherry endosomes were associated and/or overlapped with late endosomes marked by YFP-Rab7 (Fig. 3, F and G; and Video 4) and with late endosomes/lysosomes marked by GFP-Lamp1 (Fig. 3 E). Thus, endosomal GFP-fluorescent Notch was mostly detected at early/sorting endosomes, whereas Cherry-fluorescent Notch was seen, at least in part, at late acidic endosomes.

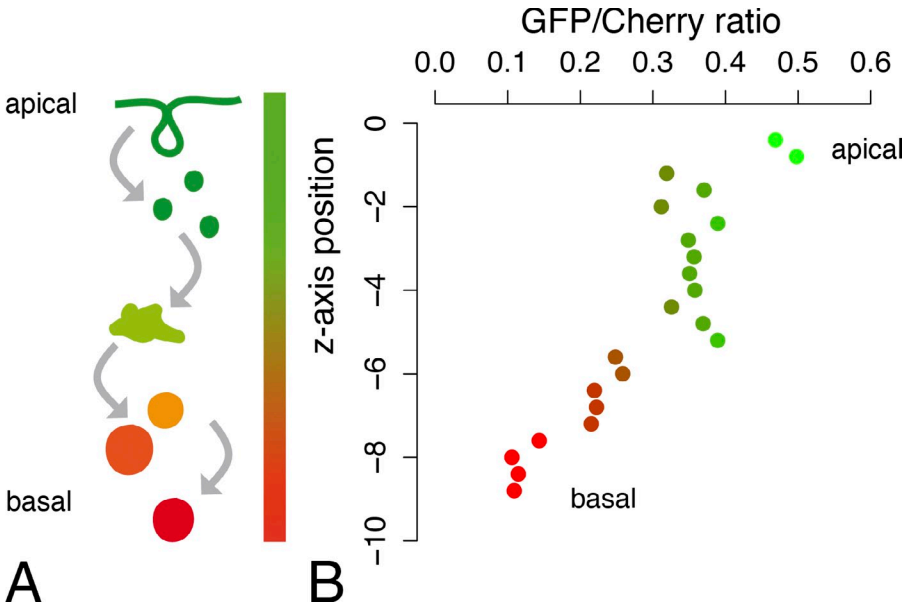

Figure 4. **Apical–basal gradient of endosomal GFP/Cherry-tagged Notch.** (A) A schematic representation of the distribution of the NiGFP4Cherry5 fluorescence along the apical–basal axis in notum epithelial cells. The GFP fluorescence of NiGFP4Cherry5 is strong at the apical plasma membrane (top, green) and in early/sorting endosomes and weak in late basal endosomes (bottom, red) as a result of quenching. Conversely, the Cherry fluorescence is weak at the plasma membrane and at early apical endosomes as a result of slow maturation time and strong in late basal endosomes. (right) This results in opposite gradients of GFP and Cherry fluorescence along the apical–basal axis. (B) The GFP/Cherry mean intensity ratios measured in endosomes were plotted along the apical–basal axis of notum epithelial cells (apical, z = 0; *n* = 4 nota; GFP- and Cherry-positive endosomes were combined to calculate mean ratio values). Ratios were calculated from raw pixel intensity values in the GFP and Cherry channels without normalization.

The aforementioned data suggested that the GFP signal of NiGFP4Cherry5 might be quenched in late acidic compartments. To test this hypothesis, the pH was increased in late endocytic compartments by disrupting the activity of the V-ATPase vacuolar proton pump using RNAi against the V-ATPase regulator Rabconnectin-3A (Rbcn-3A). Consistent with an earlier study (Yan et al., 2009), the silencing of Rbcn-3A led to the accumulation of NiGFP4Cherry5 in enlarged endosomes. Moreover, strong GFP and Cherry signals were detected in these endosomes in living pupae (Fig. 3, H and I). This indicated that the defective acidification of late endosomes prevented the quenching of GFP. To further test the quenching hypothesis, NiGFP4Cherry5 larvae were fed with chloroquine, an endosome acidification inhibitor that acts as a lysosomotropic weak base (Ohkuma and Poole, 1978; Vaccari and Bilder, 2005). This treatment led to strong GFP fluorescence and increased GFP/Cherry fluorescence ratio in wing disc cells of living third instar larvae that were directly imaged through the cuticle (Fig. 3, J–L; Nienhaus et al., 2012). We therefore conclude that the GFP fluorescence signal of NiGFP4Cherry5 is quenched in acidic late endosomes and that the low GFP, high Cherry signal seen in living cells identified Notch in late endosomes and possibly lysosomes.

Because GFP is cytosolic in the NiGFP4Cherry5 fusion receptor, quenching of GFP by acidic pH should depend on the transfer of Notch into the endosomal lumen of multivesicular bodies. To test this prediction, we studied the fluorescence pattern of NiGFP4Cherry5 in cells mutant for the *lethal(2) giant discs* (*lgd*) gene. Earlier studies showed that Notch accumulated at the surface of enlarged endosomes in *lgd* mutant cells because of its defective intraluminal transfer (Jaekel and Klein, 2006; Troost et al., 2012). Consistent with this, NiGFP-4Cherry5 accumulated at enlarged vesicles in *lgd* mutant cells and remained GFP fluorescent (Fig. 3, M and M′). We conclude that the quenching of GFP required the intraluminal transfer of NiGFP4Cherry5, indicating that GFP is quenched in the lumen of acidic endosomes. Thus, the fluorescence properties of GFP and Cherry could be used to identify distinct pools of Notch in living cells.

Opposite apical-basal gradients of GFP and Cherry fluorescence

Both maturation of Cherry and endosome acidification are continuous processes. Thus, opposite gradients of GFP and Cherry fluorescence are expected to be seen at the level of the population of GFP/Cherry-tagged Notch traveling along the endocytic path from the plasma membrane to lysosomes. In polarized epithelial cells, high GFP/low Cherry Notch should be observed at apical early/sorting endosomes and low GFP/high Cherry Notch should be detected more basally in late endosomes (Fig. 4 A). To test this idea, we measured the ratio of the GFP and Cherry fluorescence intensities of endosomes of epithelial cells in the notum of living pupae. Endosomes were automatically and sequentially detected in the GFP and Cherry channels using a 3D wavelet transform Spot Detector plugin (de Chaumont et al., 2012). For each endosome, the GFP/Cherry ratio was calculated, and the mean ratio value for a given z position was plotted along the apical–basal axis. We found that apical endosomes had a high GFP/Cherry ratio and that this ratio decreased for more basal endosomes (Fig. 4 B). This observation was fully consistent with the known apical–basal gradient of endosome maturation, from early and apical endosomes to late and basal ones (Huotari and Helenius, 2011).

Distinct pools of E-Cadherin (Cad) and Spdo are seen by GFP/Cherry tagging

The fluorescence properties of GFP and Cherry seen with NiGFP4Cherry5 are intrinsic to GFP and Cherry and could, therefore, be used more generally to study the subcellular distribution and trafficking of membrane proteins in living cells. To test this, we first studied the distribution of GFP- and Cherry-tagged versions of DE-Cad. To do so, we used functional CadGFP and

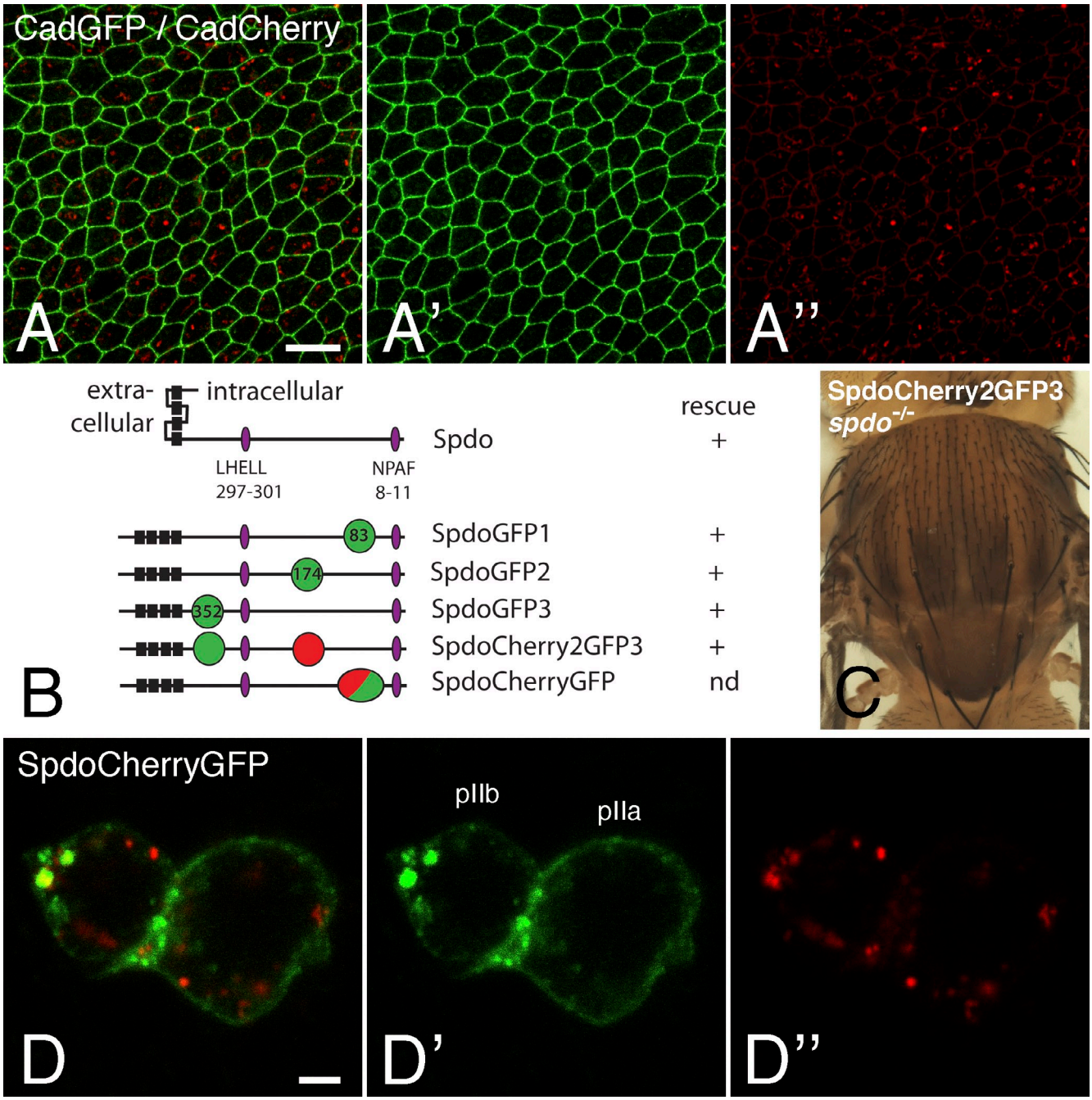

Figure 5. **Fluorescence patterns of GFP/Cherry-tagged E-Cad and Spdo.** (A–A″) Fluorescence signals produced by CadGFP (green) and CadCherry (red) in living pupae showing that GFP mostly revealed the junctional pool of E-Cad, whereas the strongest Cherry signal was detected at endosomes. Note that the junctional pool of E-Cad was also weakly Cherry positive. (B) Domain structure of Spdo showing the four transmembrane segments (black) and the LHELL and NPAF trafficking signals (purple; Tong et al., 2010; Upadhyay et al., 2013). SpdoGFP1 was described previously (Couturier et al., 2013). The points of GFP (green), Cherry (red), and GFP-Cherry tandem dimer (green and red) insertion are indicated (in amino acids). The results of the genomic rescue experiments are shown on the right. (C) *spdo* mutant flies rescued by one copy of the SpdoCherry2GFP3 BAC. (D–D″) Live imaging of SpdoCherryGFP (GFP [green] and Cherry [red]) showing that GFP and Cherry revealed distinct pools. Bars: (A) 10 µm; (D) 2 µm.

CadCherry knock-in constructs (Huang et al., 2009). A high GFP/low Cherry signal was seen at adherens junctions, whereas a low GFP/high Cherry signal was observed at endosomes of CadGFP/CadCherry trans-heterozygous pupae (Fig. 5, A–A″). We interpret these data to suggest that recently synthesized GFP-positive/Cherry-negative E-Cad were mostly present at the plasma membrane, whereas GFP-negative/Cherry-positive E-Cad mostly localized into late acidic endosomes.

We next examined the distribution of the four-pass transmembrane protein Spdo using two BAC-encoded fusion proteins, SpdoCherry2GFP3 and SpdoCherryGFP (Fig. 5, B and C). For both fusion proteins, the GFP fluorescence revealed a pool of Spdo localizing primarily at the plasma membrane and at endosomes, whereas Cherry was mostly detected at endosomes that partly overlapped with those detected by GFP (Fig. 5, D–D″; and Video 5). Again, these data were consistent

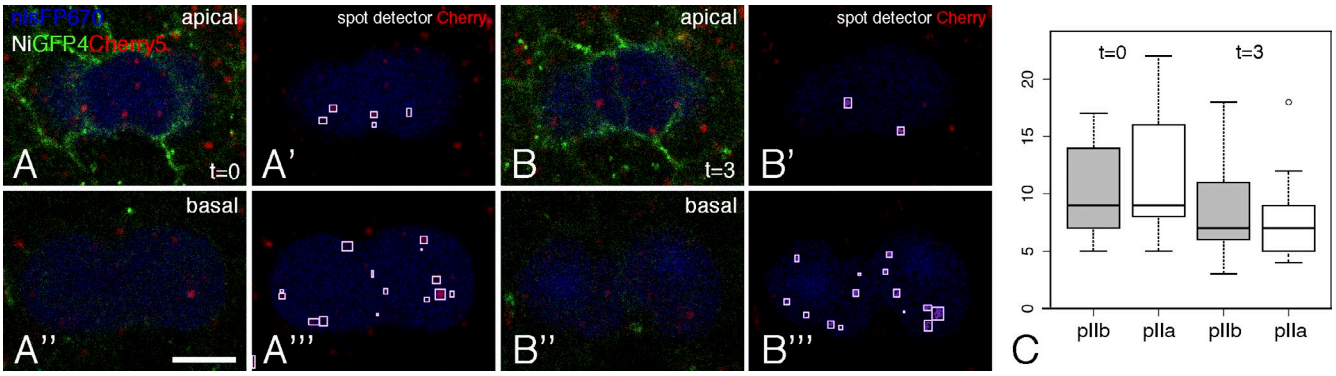

Figure 6. **Equal segregation of Notch-containing endosomes in dividing SOPs.** (A–B‴) Snapshots of a three-color video (GFP, Cherry, and *nlsFP670*, blue) showing the distribution of NiGFP4Cherry5 in mitotic SOPs (marked by *nlsFP670*) at two time points (t = 0, onset of cytokinesis, in A–A‴; t = 3 min in B–B‴). Top (apical) and bottom (basal) images show two confocal sections. Cherry-positive endosomes are shown with boxes (note that some endosomes were best detected at focal planes other than the one shown in A–B‴). Bar, 5 µm. (C) Box plot showing the number of Cherry-positive endosomes in pIIb and pIIa at t = 0 and t = 3 (n = 12; n is the number of SOPs; in this and other box plots, outliers are shown as small circles). No significant difference was observed in the number of Cherry-positive between pIIa and pIIb at t = 0 and t = 3 or between t = 0 and t = 3 in pIIb and pIIa. Box and whisker plots are uniform in their use of the box: the bottom and top of the box are the first and third quartiles, and the band inside the box is the second quartile (the median). The ends of the whiskers represent the lowest datum still within 1.5 interquartile range (IQR) of the lower quartile and the highest datum still within 1.5 IQR of the upper quartile (often called the Tukey box plot).

with GFP marking recently synthesized proteins located at the plasma membrane and early/sorting endosomes and Cherry marking mostly proteins that have been trafficked into late acidic endosomes. Thus, we propose that the GFP/Cherry tagging approach used here for Notch and Spdo should be generally useful to study the trafficking of membrane proteins in living cells and tissues.

Equal segregation of endosomal Notch in dividing SOPs

Having established the properties of NiGFP4Cherry5, it became clear that our earlier analysis of Notch distribution in living cells that was based on the fluorescence of NiGFP did not cover the late endosomal pool of Notch. We therefore reexamined the distribution of Notch in endosomes in the context of asymmetrically dividing SOPs.

Notch receptors internalized in SOPs before mitosis have been proposed to localize into endosomes marked by the protein Sara and to be directionally trafficked into the pIIa daughter cell at cytokinesis (Coumailleau et al., 2009). This conclusion was based on the live imaging of internalized anti-Notch–Fab fragment complexes in cultured notum explants. However, whether endogenous Notch is directionally trafficked into pIIa has remained unclear. Although no sign of directional trafficking was observed using GFP-tagged Notch (Couturier et al., 2012), the quenching of GFP in acidic endosomes likely prevented the detection of many Notch-containing endosomes. To circumvent this caveat, we studied the distribution of NiGFP4Cherry5 in mitotic SOPs. Because neither GFP nor Cherry markers could be used to identify SOPs without interfering with the fluorescence signals of NiGFP4Cherry5, we used the recently engineered near-infrared fluorescent protein eqFP670 (Shcherbakova and Verkhusha, 2013) to mark SOPs. The *eqFP670* sequence was fused to an NLS, and the resulting *nlsFP670* gene was expressed under the control of a SOP-specific enhancer from the *neur* gene. This allowed us to monitor the distribution of GFP- and/or Cherry-positive endosomes in mitotic SOPs at cytokinesis using three-color live imaging (Fig. 6, A–B‴; the anterior pIIb and posterior pIIa cells were identified based on n*lsFP670* expression and on their relative position; Gho and Schweisguth, 1998). First, similar numbers of Cherry-positive dots were found in pIIa and pIIb at t = 0 (early furrow ingression; in minutes) and t = 3 (complete ingression; Fig. 6 C). Second, no significant change in the number of Cherry-positive endosomes was observed between these two time points in both pIIa and pIIb ($P > 0.05$, paired t test). Also, as reported earlier for NiGFP (Couturier et al., 2012), very few GFP-positive endosomes (less than one per dividing SOP) were detected, and those appeared to distribute in both pIIa and pIIb. Although we cannot exclude that a subset of specialized endosomes containing Notch traffic directionally into pIIa at cytokinesis, our analysis showed that the bulk of Cherry-positive, Notch-containing endosomes are symmetrically segregated at cytokinesis.

pIIb-specific sorting of internalized Spdo toward late endosomes

We next investigated the endosomal sorting of Notch after the SOP division. We previously reported that GFP-tagged Notch and Spdo accumulated in apical early/sorting endosomes in pIIb (Couturier et al., 2013). Consistent with this, NiGFP and SpdoGFP1 colocalized with Cherry-Rab5 in pIIb at t = 20 (Videos 6 and 7), whereas NiCherry only weakly overlapped with GFP-Rab5, SpdoGFP1, and NumbGFP in pIIb (Videos 8–10). Thus, the fluorescence of NiGFP4Cherry5 might also be used to reveal distinct endosomes in pIIb cells, with high GFP/low Cherry endosomes corresponding to early/sorting endosomes and low GFP/high Cherry marking late endosomes. We therefore measured the total fluorescence intensity of GFP and Cherry signals in the GFP-positive (early/sorting) endosomes of pIIb at t = 15 and t = 30 after anaphase in NiGFP4Cherry5 pupae. Early/sorting endosomes were automatically detected in the GFP channel using Spot Detector, and pIIb cells were identified using

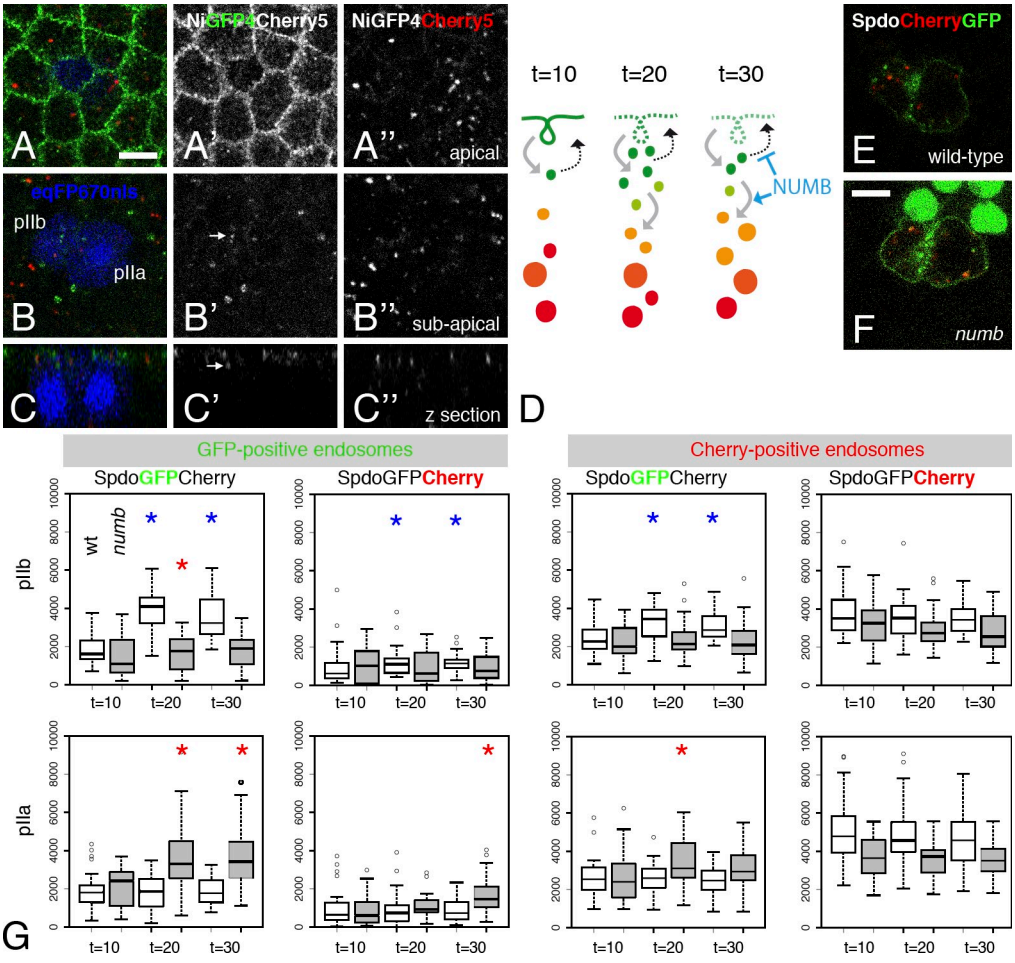

Figure 7. **pIIb-specific sorting of Spdo toward late endosomes.** (A–C″) Distribution of NiGFP4Cherry5 in SOPs (*nlsFP670*) at *t* = 15 (in minutes after anaphase). Two confocal sections (apical, A–A″; subapical, B–B″) and a transverse view (C–C″) are shown. GFP-positive endosomes are indicated with arrows in pIIb (B′ and C′). (A′) Note the low level of Notch in pIIa/pIIb cells. (D) Interpretation of the distribution of the SpdoCherryGFP fluorescence along the endocytic path in pIIb. The GFP fluorescence is initially strong at the plasma membrane of pIIb and then decreases over time as Spdo is internalized. As Spdo is endocytosed, the GFP fluorescence increases in both GFP-positive early/sorting endosomes (green endosomes) and Cherry-positive endosomes (orange and red endosomes). Numb is required to both inhibit the recycling of internalized Spdo and promote its sorting toward late endosomes. (E and F) Distribution of SpdoCherryGFP at *t* = 20 (in minutes after anaphase in wild-type and *numb* mutant clones [marked by the loss of nuclear GFP]). (F) Note the GFP fluorescence of SpdoCherryGFP at the plasma membrane of both daughter cells in the *numb* clone. (G) Box plots of the SpdoCherryGFP fluorescence intensities (GFP and Cherry, as indicated) measured in pIIb (top) and pIIa (bottom) cells in wild-type (white) and *numb* mutant cells (gray) at *t* = 10, 20, and 30 min. Total fluorescence intensities (y axis) measured in GFP-positive (early/sorting) endosomes (left) and Cherry-positive (late) endosomes (right) are shown. GFP increased significantly in the Cherry-positive endosomes of wild-type pIIb (blue asterisks indicate $P < 0.05$; see Results for p-values). Conversely, Cherry increased significantly in the GFP-positive endosomes of wild-type pIIb. Corresponding values did not significantly change in *numb* mutant cells. This indicated that GFP-positive Spdo was sorted toward late Cherry-positive endosomes in a Numb-dependent manner in pIIb. No significant changes were in wild-type pIIa. However, statistically significant changes were observed in both pIIb and pIIa in *numb* mutant clones (red asterisks indicate $P < 0.05$). These changes likely reflected the Numb-independent endocytosis of Spdo that is present at higher levels at the plasma membrane in dividing *numb* mutant SOPs. Box and whisker plots are uniform in their use of the box: the bottom and top of the box are the first and third quartiles, and the band inside the box is the second quartile (the median). The ends of the whiskers represent the lowest datum still within 1.5 IQR of the lower quartile and the highest datum still within 1.5 IQR of the upper quartile (often called the Tukey box plot). Outliers are shown as small circles. Bars, 5 µm.

the weak cytoplasmic *nlsFP670* signal (Fig. 7, A–C″). First, the endosomal GFP signal was slightly higher in pIIb than in pIIa at *t* = 15 (mean pixel intensity: 3,922 vs. 2,543; $P = 6 \times 10^{-5}$, *n* = 29). Thus, like NiGFP (Couturier et al., 2013), GFP-fluorescent NiGFP4Cherry5 localized at early/sorting endosomes in pIIb but not pIIa. Second, both GFP and Cherry fluorescence appeared to weakly increase in GFP-positive endosomes from *t* = 15 to at *t* = 30 in pIIb. Although these changes could be consistent with Notch accumulating into early/sorting endosomes and sorted toward Cherry-positive endosomes, they were not statistically significant (P = 0.35 and 0.26, respectively). Of note, the limited number, small size, and weak intensity of the GFP-positive, Notch-containing endosomes (Fig. 7, A–C″), likely caused by the SOP-specific down-regulation of Notch by Spdo (Couturier et al., 2012), made the quantitative analysis of Notch sorting in pIIb particularly difficult. Thus, better tools are needed to follow the sorting of Notch toward late endosomes in pIIb.

We therefore focused our analysis on Spdo and monitored the sorting of SpdoCherryGFP in pIIa and pIIb cells (Fig. 7 E). The GFP fluorescence measured in the GFP-positive

(early/sorting) endosomes (detected automatically in the green channel) significantly increased from $t = 10$ to $t = 20$ in pIIb ($P = 4 \times 10^{-7}$, $n = 31$; Fig. 7 G). This confirmed that Spdo is internalized from the plasma membrane soon after division to accumulate into early/sorting endosomes between $t = 10$ and $t = 20$ in pIIb cells. A slight decrease was also observed between $t = 20$ and $t = 30$. This could reflect the recycling of Spdo and/or GFP quenching associated with its sorting toward late endosomes. Consistent with the latter, the intensity of Cherry measured in GFP-positive (early/sorting) endosomes also increased over time in pIIb ($P = 0.01$; Fig. 7 G). Similarly, the intensity of GFP measured in Cherry-positive (late) endosomes increased over time ($P = 10^{-5}$; Fig. 7 G, note that GFP-positive and Cherry-positive endosomes overlapped with the detection parameters used here). In contrast, the Cherry fluorescence measured in Cherry-positive endosomes was unchanged ($P = 0.07$; Fig. 7 G). Finally, the GFP and Cherry signals remained constant over time in the GFP- and Cherry-positive endosomes in pIIa ($P > 0.3$; Fig. 7 G). We interpret these results to suggest that internalized GFP-positive Spdo was in part trafficked toward Cherry-positive (late) endosomes (Fig. 7 D). This proposed sorting of internalized Spdo toward late endosomes was pIIb specific.

We next examined the role of *numb* in the sorting of SpdoCherryGFP (Fig. 7 F). In contrast to wild-type pIIb cells, no increase of GFP signal was detected in the Cherry-positive endosomes of *numb* mutant pIIb cells ($n = 27$; Fig. 7 G). Likewise, no increase of Cherry signal was measured in the GFP-positive endosomes of *numb* mutant pIIb cells. We therefore conclude that the sorting of internalized GFP-positive Spdo into late Cherry-positive endosomes depends on the activity of the *numb* gene.

Together, our results indicated that internalized Spdo was rapidly sorted toward late endosomes in pIIb but not pIIa, suggesting that Numb may regulate the endosomal sorting of internalized Spdo in pIIb. More generally, this analysis indicated that dual-tagged sensors might be used to quantitatively study the sorting of membrane proteins in vivo.

Discussion

Recent advances in the characterization of fluorescent proteins have contributed to the design of new tools to study the dynamics of various biological processes in living cells. For instance, the difference in pH sensitivity between GFP and Cherry was used to monitor endosome fission (Merrifield et al., 2005) and autophagy (Kimura et al., 2007). Also, the difference in maturation kinetics between GFP and Cherry was used to measure protein turnover (Khmelinskii et al., 2012; Donà et al., 2013). Here, we have shown that GFP- and Cherry-tagged Notch and Spdo exhibited distinct fluorescence patterns, with high GFP/low Cherry signals at the plasma membrane and low GFP/high Cherry signals in acidic endosomes. The slow maturation of Cherry relative to GFP may explain the low Cherry fluorescence at the plasma membrane seen for Notch, Spdo, and, to a lesser extent, E-Cad. In support of this interpretation, stabilization of Notch at the plasma membrane in *krz* mutant cells allowed the detection of the Cherry signal of NiCherry, i.e., stabilization of NiCherry gave Cherry enough time to mature. In addition, the quenching of GFP by low pH likely accounts for the lack of GFP fluorescence produced by dual-tagged sensors in late acidic endosomes. In support of this interpretation, we showed that the inhibition of endosome acidification, by silencing *Rbcn-3A* or titrating the pH upwards using chloroquine, restored GFP fluorescence. In principle, changes in the relative fluorescence within a pair of chromophores might also result from Forster resonance energy transfer (FRET), a phenomenon that can be used to probe conformation change. However, FRET is unlikely to contribute to the differences reported in this study for GFP and Cherry because differences between GFP and Cherry fluorescence were observed (a) for three structurally unrelated proteins, Notch, Spdo, and E-Cad; (b) for pairs of chromophores carried either together on a single molecule (NiGFP4Cherry5) or separately on two distinct molecules (NiGFP and NiCherry); (c) for tags inserted at different positions within the protein sequence (SpdoCherryGFP and SpdoCherry2GFP3); and (d) for a Cherry–superfolder GFP (sfGFP) tandem dimer that produced no significant FRET signal (Khmelinskii et al., 2012). Thus, the combination of slow maturation time of Cherry (relative to GFP) and pH sensitivity of GFP (relative to Cherry) allowed us to monitor the path followed by Notch and Spdo from the plasma membrane to late acidic endosomes.

One major and general implication of our study is that GFP is not a good marker to study the distribution of membrane proteins into endocytic compartments. Specifically, only a fraction of the endosomal pool of Notch and Spdo could be detected using GFP, indicating that the NiGFP and SpdoGFP1 fluorescence signals did not faithfully report on the presence of these proteins in late endosomes (Couturier et al., 2012, 2013).

Our data not only suggested that the results of protein distribution should be interpreted with care when using GFP- and Cherry-fluorescent proteins but also indicated that these differences may be exploited to learn about the journey of these tagged proteins within living cells because GFP/Cherry-tagged proteins with a rapid turnover should be GFP high/Cherry low in early/sorting endosomes and GFP low/Cherry high in acidic endosomes. Thus, dual-tagged sensors could be used very generally to study trafficking dynamics of membrane proteins.

However, this approach requires tagging the cargo of interest. Moreover, tagging should not interfere with the activity and trafficking of the considered cargo. Here, we have used sequence divergence across related species to define points of fusion, BAC-encoded transgene to achieve proper gene expression, and genomic rescue assays to test for function (Couturier et al., 2012, 2013). Recent advances in CRISPR (clustered regularly interspaced short palindromic repeats)-mediated genome engineering should simplify this step and make it more generally applicable (Hsu et al., 2014). This approach also requires two channels for simultaneous acquisition in living cells. Therefore, fluorescent markers with emission spectra distinct from those of GFP and Cherry may be needed to locate the dual-tagged cargo relative to subcellular structures and/or specific cells within complex tissues. Here, we have shown that the near–infra red fluorescent protein eqFP670 can be used for this purpose (Shcherbakova and Verkhusha, 2013): three-color imaging

with high temporal and spatial resolution allowed us to monitor the partitioning of Notch at mitosis. Thus, dual-tagged sensors are likely to be of general interest for the analysis of membrane protein trafficking in model organisms.

Dual-tagged sensors were used here to study the distribution and trafficking of Notch and Spdo in asymmetrically dividing SOPs by live imaging. We first used GFP/Cherry-tagged Notch to show that Notch-containing endosomes are equally inherited by SOP daughter cells. Thus, our observation did not support a model proposing that the pIIa/pIIb fate decision is in part regulated by the directional trafficking of a specific endosomal pool of Notch (Coumailleau et al., 2009). The basis for this discrepancy remains to be explained. We next used GFP/Cherry-tagged Spdo to study endosomal sorting. Endosome maturation is both accompanied and driven by luminal acidification (Huotari and Helenius, 2011). Thus, it should be possible to follow this process in real time by monitoring the GFP/Cherry ratio over time. However, differences in bleaching rate between GFP and Cherry under our imaging conditions prevented us from adopting this imaging strategy. Vesicle fusion also contributes to endosome maturation. However, fusion events involving small and rapidly moving endosomes could not be detected, owing to the relatively limited temporal–spatial resolution of our imaging conditions, and only fusion of large endosomes was occasionally observed. Also, fusion of GFP-positive endosomes to larger Cherry-positive acidic compartments may escape detection as a result of the rapid quenching of GFP. We therefore monitored sorting by measuring GFP and Cherry fluorescence levels in both GFP-positive (early/sorting) endosomes and Cherry-positive (late) endosomes at defined time points. This approach provided in vivo evidence that Spdo is sorted toward late endosomes in pIIb cells. Specifically, we showed that GFP-positive SpdoCherryGFP rapidly accumulated into the early/sorting endosomes of pIIb (but not those of pIIa), confirming earlier findings (O'Connor-Giles and Skeath, 2003; Hutterer and Knoblich, 2005; Langevin et al., 2005; Tong et al., 2010; Cotton et al., 2013; Couturier et al., 2013). We also found that a fraction of internalized GFP-positive Spdo was sorted toward Cherry-positive (late) endosomes and that this sorting was Numb dependent. We therefore propose that Numb not only inhibits the recycling of Spdo (Cotton et al., 2013; Couturier et al., 2013) but also promotes the sorting of internalized Spdo toward late endosomes, as initially proposed for the regulation of Notch by Numb in mammalian cells (McGill et al., 2009). In conclusion, we have shown that dual-tagged sensors can be used to study the sorting dynamics of membrane proteins in *Drosophila* and have provided in vivo evidence that internalized Spdo is sorted toward late endosomes in Numb-inheriting cells in the context of asymmetric cell division.

Materials and methods

Flies

The following mutant and transgenic flies were used: NiGFP (a BAC-encoded, GFP-tagged version of Notch; GFP was inserted in the intracellular domain at position 5; Fig. 1 A; Couturier et al., 2012), SpdoGFP (a BAC-encoded, GFP-tagged version of Spdo; GFP was inserted in the intracellular region at position 1 and was therefore renamed SpdoGFP1; Fig. 5 B; Couturier et al., 2013), Cherry-Rab5 (a genomic construct carrying Cherry fused to the N terminus of Rab5 with a TRGGGGG linker; obtained from R. DeLotto, University of Copenhagen, Copenhagen, Denmark; Lund et al., 2010), EGFP-Rab5 (a knock-in allele of Rab5 generated by homologous recombination; obtained from S. De Renzis, European Molecular Biology Laboratory, Heidelberg, Germany; Fabrowski et al., 2013), pTub-Cherry-Rab4 (a transgene expressing a Cherry-Rab4 fusion downstream of a *tubulin* promoter; obtained from T. Klein, European Molecular Biology Laboratory, Heidelberg, Germany; Yousefian et al., 2013), pTub-GFP-LAMP1 (a transgene expressing extracellular EGFP fused to a transmembrane domain and cytoplasmic tail of human LAMP1 under the control of the ubiquitous *tubulin* promoter; this cytoplasmic tail is sufficient to direct the protein produced to late endosomes and lysosomes in *Drosophila*; obtained from H. Krämer, University of Texas Southwestern, Dallas, TX; Akbar et al., 2009), pTub-YFP-Rab7 and pTub-YFP-Rab11 (transgenes expressing YFP fused to Rab7, or Rab11, under the control of the ubiquitous *tubulin* promoter; both obtained from S. Eaton, Max Planck Institute of Molecular Cell Biology and Genetics, Dresden, Germany; Marois et al., 2006), neur-PH-RFP (a transgene expressing the pleckstrin homology domain of PLCδ1 fused to mRFP1 under the control of a SOP-specific enhancer from the *neur* gene; Couturier et al., 2013), E-Cad–GFP and E-Cad–Cherry (knock-in alleles of the *shotgun* gene that encodes E-Cad; obtained from Y. Hong, University of Pittsburgh, Pittsburgh, PA; Huang et al., 2009), N^{55e11} (a null allele of *Notch*) *Ubx-flp* (a transgene expressing the flippase under the control of *Ubx* regulatory element; obtained from J. Knoblich, Institute of Molecular Biotechnology, Vienna, Austria; Hutterer and Knoblich, 2005), *FRT40A* lgd^{d7} (a null allele of *lgd*; obtained from T. Klein; Jaekel and Klein, 2006), *FRT40A* $numb^{15}$ (a null allele of *numb* obtained from J. Knoblich; Berdnik and Knoblich, 2002; a *fat* mutant allele was removed from the original chromosome by recombination; Couturier et al., 2012), *FRT82B* krz^{1} (a mutant allele of *krz* obtained from T. Klein; Mukherjee et al., 2005), *FRT40A ubi-nlsGFP* (a nuclear GFP marker on chromosome 2L), *FRT40A ubi-nlsRFP* (a nuclear RFP marker on chromosome 2L), *FRT82B ubi-nlsRFP* (a nuclear RFP marker on chromosome 3R), *ap-Gal4* (an enhancer-trap expressing GAL4 under the control of the *ap* gene), *pTub-Gal80*^{ts} (a transgene expressing a thermosensitive version of GAL80, a repressor of GAL4, under the control of the tubulin promoter), and UAS (upstream activating sequence)-dsRNA *Rbcn-3A* (P{TRiP.HMS01287}attP2; a transgene expressing a double-stranded RNA directed against the *Rbcn-3A* gene; Ni et al., 2011). Chloroquine (Sigma-Aldrich) was mixed in food-containing larvae at a final 10-mM concentration.

Transgenes

The attB-P[acman]-ApR *Notch* clone (Couturier et al., 2012) and the attB-P[acman]-Cmr CH322-119I20 (*spdo*) BACs (Couturier et al., 2013) were used to generate transgenic flies. These BACs were further modified using recombineering-mediated gap repair (Venken et al., 2006) using the following primers: For NiCherry, the Cherry sequence was introduced at position 5 using homology arms as described previously for NiGFP (Couturier et al., 2012). NiGFP4Cherry5 was obtained from NiCherry using notchgfp4 forward, 5′-ACGGGGGGAGTGTCGGGCGTGCCGGGTGTAggtatggtgagcaagggcga-3′; and notchgfp4 reverse, 5′-AGCTGCTTGTGCCGCTGAATTCGTTGGCGGaacaccaacaccctgtaca-3′. SpdoGFP2 and SpdoGFP3 were obtained as described previously for SpdoGFP (Couturier et al., 2013; noted here SpdoGFP1) using spdoigfp2 forward, 5′-CAGTTTGCCAGCTTGCCACCGATACTTAATggtgttggcatggtgagcaagggcg-3′; spdoigfp2 reverse, 5′-GTTGTTAATATTCCTGGGCTTGGGCGGCAAgccaacaccttgtacagctcgtcc-3′; spdoigfp3 forward, 5′-CAAAGCCAACAAGTTGGAGCGGTAGTAGGAgttggcatggtgagcaagggcgagg-3′; and spdoigfp3 reverse, 5′-ATTCTGGCGAAGTGGCAAGGTTGGAGGGACgccaacaccttgtacagctcgtcc-3′. SpdoCherry2GFP3 was obtained from SpdoGFP3 using spdocherryi2 forward, 5′-CAGTTTGCCAGCTTGCCACCGATACTTAATggtgttggcatggtgagcaagggcgaggagg-3′; and spdocherryi2 reverse, 5′-GTTGTTAATATTCCTGGGCTTGGGCGGCAAgccaacaccttgtacagctcgtccatgccg-3′. (Uppercase letters correspond to the homology arms for recombination with the BAC DNA; lowercase letters correspond to the sequence priming the PCR amplification reaction to produce the recombination donor DNA.) For SpdoCherryGFP, the sequence of the Cherry-sfGFP tandem dimer (provided by M. Knop, University of Heidelberg, Heidelberg, Germany; Khmelinskii et al., 2012) was codon optimized for *Drosophila* and synthesized in vitro and used as a template for PCR amplification using the following primers to perform recombineering: spdoCh-sfGfpi forward, 5′-CAGCAGCAGCAGCAGCAGCAACACCAACAGggggttggcatggtgagcaagggcg-3′; and spdoCh-sfGfpi1 reverse, 5′-CTGCTGAGCCAGGTGTTGCTGGTGTATCTGgccaacaccggatcccttgtac-3′. For *neur-nlsFP670*, the

sequence of the *eqFP670* gene (Shcherbakova and Verkhusha, 2013) was codon optimized and fused in frame downstream of an NLS from mouse CBP80, and the resulting gene was synthesized in vitro to generate the *nlsFP670* gene. The latter was inserted into the Stinger-attB-p*neur*-GFP plasmid (provided by S. Aerts, KU Leuven, Leuven, Belgium; Aerts et al., 2010) to replace GFP.

All constructs were verified by sequencing the recombined regions before phiC31-mediated integration. The resulting transgenes were integrated at the following attP sites: M[p3×P3-RFP, attP]51D (NiCherry), PB[y$^+$ attP-9A]VK19 at position 68D2 (NiGFP4Cherry5), P{CaryP}attP2 at position 68A4 (SpdoGFP2, SpdoGFP3, and SpdoCherry2GFP3), PB[y$^+$ attP-9A]VK20 at position 99F8 (SpdoCherryGFP), and PB[y$^+$ attP-3B]VK02 at position 28E7 (*neur-nlsFP670*). BAC injection was performed by BestGene, Inc.

Genomic rescue assays were performed as described previously (Couturier et al., 2012, 2013): Autosomal NiCherry and NiGFP4Cherry5 transgenes were combined with the X-linked N^{55e11} mutation, and rescue was studied in males carrying one copy of the transgene. The SpdoGFP2, SpdoGFP3, SpdoCherry2GFP3 transgenes were recombined with the $spdo^{ZZ27}$ deletion, and rescue was tested in $spdo^{ZZ27}/spdo^{G104}$ flies.

Immunostaining, microscopy, and image analysis

Dissection of staged pupae and antibody staining were performed using standard procedures. In brief, nota were dissected from staged pupae using Vannas Micro-Scissors, fixed in paraformaldehyde (4% in PBS), and incubated in PBT (PBS with 0.1% Triton X-100). The following antibodies were used: goat anti-GFP (1:500; Abcam), rabbit anti-DsRed (1:200; Takara Bio Inc.), and mouse anti-NICD (1:100; C17 9C6; Developmental Studies Hybridoma Bank). Secondary antibodies were obtained from Jackson ImmunoResearch Laboratories, Inc. After washes in PBT, nota were mounted in 4% *N*-propyl-gallate and 80% glycerol.

Wing discs were imaged through the cuticle of living third instar larvae as previously described in Nienhaus et al. (2012). In brief, living larvae were placed in a drop of water deposited on a slide between two coverslips and then immobilized by a coverslip put on top on this montage. Imaging was performed using a microscope (DMRXA; Leica) equipped with a spinning disk (CSU-X1; Yokogawa Electric Corporation), a back-illuminated camera (QuantEM 512C; Photometrics), 491/561-nm lasers, and a 40× (HCX Plan Apochromat CS, NA 1.4) objective. Acquisition was performed using the MetaMorph software (Molecular Devices). The GFP/Cherry ratio shown in Fig. 3 J was calculated over a field of cells covering the wing pouch (n = 5 discs).

Live imaging of pupae was performed as described previously (Couturier et al., 2012). In brief, staged pupae were transferred onto a microscope slide with a double-sided tape between two spacers. The pupal case was removed using forceps, and a coverslip coated with Voltalef oil was deposited onto the spacers (Couturier and Schweisguth, 2014). Imaging was performed using a confocal microscope (LSM 780; Carl Zeiss) with a 63× (Plan Apochromat, NA 1.4 differential interference contrast M27) objective and 488 (GFP)-, 514 (YFP)-, 561 (RFP and Cherry)-, and 633 (eqFP670)-nm lasers. The GFP and Cherry signals were always acquired simultaneously.

GFP- and Cherry-positive endosomes were independently identified and defined using the 3D wavelet transform Spot Detector plugin under Icy (de Chaumont et al., 2012). Parameters were set at 30–80 (threshold scale 2) and 25–100 (minimum size, in pixels). Results were exported into Excel (Microsoft) for analysis. The absolute values of the GFP/Cherry ratios varied depending on laser intensity settings. Because the intensity of the He/Ne 488-nm laser was set manually, all ratio data shown in this study were acquired within the same confocal session.

Statistical significance was tested using paired *t* tests when data distribution followed a normal law (Shapiro test). In all other cases, a non-parametric sign test under R was used.

Western blots

Wing imaginal discs were dissected from 30 third instar larvae, and protein extracts were prepared in a 50 mM Tris, pH 8, 150 mM NaCl, and 1% NP-40 buffer. Protein concentration was determined using a spectrophotometer (NanoDrop1000; Thermo Fisher Scientific), and 20 µg protein was loaded per lane on 4–20% precast Mini-PROTEAN TGX gels for SDS-PAGE. Proteins were transferred onto 0.2-µm nitrocellulose membranes (Bio-Rad Laboratories). The following primary antibodies were used: rabbit anti-GFP (1:4,000; Molecular Probes), rabbit anti-DsRed (1:4,000), and mouse anti-NICD (C17 9C6; 1:2,000). HRP-coupled anti–mouse/rabbit antibodies (1:10,000; GE Healthcare) were detected using a chemiluminescent substrate (SuperSignal West Femto; Thermo Fisher Scientific).

Online supplemental material

Fig. S1 presents results from a Western blot analysis of GFP- and/or Cherry-tagged Notch. Table S1 details all genotypes studied here. Video 1 shows localization of NiGFP and Cherry-Rab5 in notum epithelial cells. Video 2 shows localization of NiGFP and Cherry-Rab4 in notum epithelial cells. Video 3 shows localization of NiCherry and GFP-Rab5 in notum epithelial cells. Video 4 shows localization of NiCherry and YFP-Rab7 in notum epithelial cells. Video 5 shows localization of SpdoCherryGFP in pIIa/pIIb cells. Video 6 shows localization of NiGFP and Cherry-Rab5 in pIIa/pIIb cells. Video 7 shows localization of SpdoGFP1 and Cherry-Rab5 in pIIa/pIIb cells. Video 8 shows localization of NiCherry and GFP-Rab5 in pIIa/pIIb cells. Video 9 shows localization of NiCherry and SpdoGFP in pIIb. Video 10 shows localization of NiCherry and Numb-GFP in pIIb. Online supplemental material is available at http://www.jcb.org/cgi/content/full/jcb.201407071/DC1.

We thank S. Aerts, R. Bodmer, R. DeLotto, S. De Renzis, S. Eaton, Y. Hong, T. Klein, J. Knoblich, M. Knop, H. Krämer, J. Skeath, the Bloomington Drosophila Stock Center, Drosophila Genetic Research Center, Drosophila Genomics Resource Center, and FlyBase for flies, antibodies, DNA, software, and other resources. We thank N. Vodovar who generated the NiCherry flies and F. De Chaumont and N. Chenouard for help with Icy. We thank H. Krämer, R. Le Borgne, and all laboratory members for advice and discussion.

This work was funded by grants from the Fondation pour la Recherche Médicale (DEQ20100318284) and Agence Nationale pour la Recherche (Labex Revive).

The authors declare no competing financial interests.

Submitted: 16 July 2014
Accepted: 24 September 2014

References

Aerts, S., X.J. Quan, A. Claeys, M. Naval Sanchez, P. Tate, J. Yan, and B.A. Hassan. 2010. Robust target gene discovery through transcriptome perturbations and genome-wide enhancer predictions in *Drosophila* uncovers a regulatory basis for sensory specification. *PLoS Biol.* 8:e1000435. http://dx.doi.org/10.1371/journal.pbio.1000435

Akbar, M.A., S. Ray, and H. Krämer. 2009. The SM protein Car/Vps33A regulates SNARE-mediated trafficking to lysosomes and lysosome-related organelles. *Mol. Biol. Cell*. 20:1705–1714. http://dx.doi.org/10.1091/mbc.E08-03-0282

Berdnik, D., and J.A. Knoblich. 2002. *Drosophila* Aurora-A is required for centrosome maturation and actin-dependent asymmetric protein localization during mitosis. *Curr. Biol.* 12:640–647. http://dx.doi.org/10.1016/S0960-9822(02)00766-2

Berdnik, D., T. Török, M. González-Gaitán, and J.A. Knoblich. 2002. The endocytic protein α-Adaptin is required for numb-mediated asymmetric cell division in *Drosophila*. *Dev. Cell*. 3:221–231. http://dx.doi.org/10.1016/S1534-5807(02)00215-0

Collinet, C., M. Stöter, C.R. Bradshaw, N. Samusik, J.C. Rink, D. Kenski, B. Habermann, F. Buchholz, R. Henschel, M.S. Mueller, et al. 2010. Systems survey of endocytosis by multiparametric image analysis. *Nature*. 464:243–249. http://dx.doi.org/10.1038/nature08779

Cotton, M., N. Benhra, and R. Le Borgne. 2013. Numb inhibits the recycling of Sanpodo in *Drosophila* sensory organ precursor. *Curr. Biol.* 23:581–587. http://dx.doi.org/10.1016/j.cub.2013.02.020

Coumailleau, F., M. Fürthauer, J.A. Knoblich, and M. González-Gaitán. 2009. Directional Delta and Notch trafficking in Sara endosomes during asymmetric cell division. *Nature*. 458:1051–1055. http://dx.doi.org/10.1038/nature07854

Couturier, L., and F. Schweisguth. 2014. Antibody uptake assay and in vivo imaging to study intracellular trafficking of Notch and Delta in *Drosophila*. *Methods Mol. Biol.* 1187:79–86. http://dx.doi.org/10.1007/978-1-4939-1139-4_6

Couturier, L., N. Vodovar, and F. Schweisguth. 2012. Endocytosis by Numb breaks Notch symmetry at cytokinesis. *Nat. Cell Biol.* 14:131–139. http://dx.doi.org/10.1038/ncb2419

Couturier, L., K. Mazouni, and F. Schweisguth. 2013. Numb localizes at endosomes and controls the endosomal sorting of notch after asymmetric division in *Drosophila*. *Curr. Biol.* 23:588–593. http://dx.doi.org/10.1016/j.cub.2013.03.002

de Chaumont, F., S. Dallongeville, N. Chenouard, N. Hervé, S. Pop, T. Provoost, V. Meas-Yedid, P. Pankajakshan, T. Lecomte, Y. Le Montagner, et al. 2012. Icy: an open bioimage informatics platform for extended reproducible research. *Nat. Methods*. 9:690–696. http://dx.doi.org/10.1038/nmeth.2075

Doherty, G.P., K. Bailey, and P.J. Lewis. 2010. Stage-specific fluorescence intensity of GFP and mCherry during sporulation in bacillus subtilis. *BMC Res. Notes*. 3:303.

Donà, E., J.D. Barry, G. Valentin, C. Quirin, A. Khmelinskii, A. Kunze, S. Durdu, L.R. Newton, A. Fernandez-Minan, W. Huber, et al. 2013. Directional tissue migration through a self-generated chemokine gradient. *Nature*. 503:285–289.

Fabrowski, P., A.S. Necakov, S. Mumbauer, E. Loeser, A. Reversi, S. Streichan, J.A. Briggs, and S. De Renzis. 2013. Tubular endocytosis drives remodelling of the apical surface during epithelial morphogenesis in *Drosophila*. *Nat. Commun.* 4:2244. http://dx.doi.org/10.1038/ncomms3244

Gho, M., and F. Schweisguth. 1998. Frizzled signalling controls orientation of asymmetric sense organ precursor cell divisions in *Drosophila*. *Nature*. 393:178–181. http://dx.doi.org/10.1038/30265

Gho, M., Y. Bellaïche, and F. Schweisguth. 1999. Revisiting the *Drosophila* microchaete lineage: a novel intrinsically asymmetric cell division generates a glial cell. *Development*. 126:3573–3584.

Hartenstein, V., and J.W. Posakony. 1989. Development of adult sensilla on the wing and notum of *Drosophila melanogaster*. *Development*. 107: 389–405.

Hartenstein, V., and J.W. Posakony. 1990. A dual function of the Notch gene in *Drosophila* sensillum development. *Dev. Biol.* 142:13–30. http://dx.doi.org/10.1016/0012-1606(90)90147-B

Hebisch, E., J. Knebel, J. Landsberg, E. Frey, and M. Leisner. 2013. High variation of fluorescence protein maturation times in closely related *Escherichia coli* strains. *PLoS ONE*. 8:e75991. http://dx.doi.org/10.1371/journal.pone.0075991

Hsu, P.D., E.S. Lander, and F. Zhang. 2014. Development and applications of CRISPR-Cas9 for genome engineering. *Cell*. 157:1262–1278. http://dx.doi.org/10.1016/j.cell.2014.05.010

Huang, J., W. Zhou, W. Dong, A.M. Watson, and Y. Hong. 2009. From the Cover: Directed, efficient, and versatile modifications of the *Drosophila* genome by genomic engineering. *Proc. Natl. Acad. Sci. USA*. 106:8284–8289. http://dx.doi.org/10.1073/pnas.0900641106

Huotari, J., and A. Helenius. 2011. Endosome maturation. *EMBO J.* 30:3481–3500. http://dx.doi.org/10.1038/emboj.2011.286

Hutterer, A., and J.A. Knoblich. 2005. Numb and α-Adaptin regulate Sanpodo endocytosis to specify cell fate in *Drosophila* external sensory organs. *EMBO Rep.* 6:836–842. http://dx.doi.org/10.1038/sj.embor.7400500

Iizuka, R., M. Yamagishi-Shirasaki, and T. Funatsu. 2011. Kinetic study of de novo chromophore maturation of fluorescent proteins. *Anal. Biochem.* 414:173–178. http://dx.doi.org/10.1016/j.ab.2011.03.036

Jaekel, R., and T. Klein. 2006. The *Drosophila* Notch inhibitor and tumor suppressor gene lethal (2) giant discs encodes a conserved regulator of endosomal trafficking. *Dev. Cell*. 11:655–669. http://dx.doi.org/10.1016/j.devcel.2006.09.019

Kandachar, V., and F. Roegiers. 2012. Endocytosis and control of Notch signaling. *Curr. Opin. Cell Biol.* 24:534–540. http://dx.doi.org/10.1016/j.ceb.2012.06.006

Khmelinskii, A., P.J. Keller, A. Bartosik, M. Meurer, J.D. Barry, B.R. Mardin, A. Kaufmann, S. Trautmann, M. Wachsmuth, G. Pereira, et al. 2012. Tandem fluorescent protein timers for in vivo analysis of protein dynamics. *Nat. Biotechnol.* 30:708–714. http://dx.doi.org/10.1038/nbt.2281

Kimura, S., T. Noda, and T. Yoshimori. 2007. Dissection of the autophagosome maturation process by a novel reporter protein, tandem fluorescent-tagged LC3. *Autophagy*. 3:452–460. http://dx.doi.org/10.4161/auto.4451

Kneen, M., J. Farinas, Y. Li, and A.S. Verkman. 1998. Green fluorescent protein as a noninvasive intracellular pH indicator. *Biophys. J.* 74:1591–1599. http://dx.doi.org/10.1016/S0006-3495(98)77870-1

Krieger, J.R., P. Taylor, A.S. Gajadhar, A. Guha, M.F. Moran, and C.J. McGlade. 2013. Identification and selected reaction monitoring (SRM) quantification of endocytosis factors associated with Numb. *Mol. Cell. Proteomics*. 12:499–514. http://dx.doi.org/10.1074/mcp.M112.020768

Lai, E.C., G.A. Deblandre, C. Kintner, and G.M. Rubin. 2001. *Drosophila* neuralized is a ubiquitin ligase that promotes the internalization and degradation of delta. *Dev. Cell*. 1:783–794. http://dx.doi.org/10.1016/S1534-5807(01)00092-2

Langevin, J., R. Le Borgne, F. Rosenfeld, M. Gho, F. Schweisguth, and Y. Bellaïche. 2005. Lethal giant larvae controls the localization of notch-signaling regulators numb, neuralized, and Sanpodo in *Drosophila* sensory-organ precursor cells. *Curr. Biol.* 15:955–962. http://dx.doi.org/10.1016/j.cub.2005.04.054

Le Borgne, R., and F. Schweisguth. 2003. Unequal segregation of Neuralized biases Notch activation during asymmetric cell division. *Dev. Cell*. 5:139–148. http://dx.doi.org/10.1016/S1534-5807(03)00187-4

Le Borgne, R., A. Bardin, and F. Schweisguth. 2005. The roles of receptor and ligand endocytosis in regulating Notch signaling. *Development*. 132:1751–1762. http://dx.doi.org/10.1242/dev.01789

Lund, V.K., Y. DeLotto, and R. DeLotto. 2010. Endocytosis is required for Toll signaling and shaping of the Dorsal/NF-κB morphogen gradient during *Drosophila* embryogenesis. *Proc. Natl. Acad. Sci. USA*. 107:18028–18033. http://dx.doi.org/10.1073/pnas.1009157107

Macdonald, P.J., Y. Chen, and J.D. Mueller. 2012. Chromophore maturation and fluorescence fluctuation spectroscopy of fluorescent proteins in a cell-free expression system. *Anal. Biochem.* 421:291–298. http://dx.doi.org/10.1016/j.ab.2011.10.040

Marois, E., A. Mahmoud, and S. Eaton. 2006. The endocytic pathway and formation of the Wingless morphogen gradient. *Development*. 133:307–317. http://dx.doi.org/10.1242/dev.02197

McGill, M.A., S.E. Dho, G. Weinmaster, and C.J. McGlade. 2009. Numb regulates post-endocytic trafficking and degradation of Notch1. *J. Biol. Chem.* 284:26427–26438. http://dx.doi.org/10.1074/jbc.M109.014845

Merrifield, C.J., D. Perrais, and D. Zenisek. 2005. Coupling between clathrin-coated-pit invagination, cortactin recruitment, and membrane scission observed in live cells. *Cell*. 121:593–606. http://dx.doi.org/10.1016/j.cell.2005.03.015

Merzlyak, E.M., J. Goedhart, D. Shcherbo, M.E. Bulina, A.S. Shcheglov, A.F. Fradkov, A. Gaintzeva, K.A. Lukyanov, S. Lukyanov, T.W. Gadella, and D.M. Chudakov. 2007. Bright monomeric red fluorescent protein with an extended fluorescence lifetime. *Nat. Methods*. 4:555–557. http://dx.doi.org/10.1038/nmeth1062

Mukherjee, A., A. Veraksa, A. Bauer, C. Rosse, J. Camonis, and S. Artavanis-Tsakonas. 2005. Regulation of Notch signalling by non-visual β-arrestin. *Nat. Cell Biol.* 7:1191–1201. http://dx.doi.org/10.1038/ncb1327

Ni, J.-Q., R. Zhou, B. Czech, L.-P. Liu, L. Holderbaum, D. Yang-Zhou, H.-S. Shim, R. Tao, D. Handler, P. Karpowicz, et al. 2011. A genome-scale shRNA resource for transgenic RNAi in *Drosophila*. *Nat. Methods*. 8:405–407. http://dx.doi.org/10.1038/nmeth.1592

Nienhaus, U., T. Aegerter-Wilmsen, and C.M. Aegerter. 2012. In-vivo imaging of the *Drosophila* wing imaginal disc over time: novel insights on growth and boundary formation. *PLoS ONE*. 7:e47594. http://dx.doi.org/10.1371/journal.pone.0047594

Nilsson, L., B. Conradt, A.F. Ruaud, C.C. Chen, J. Hatzold, J.L. Bessereau, B.D. Grant, and S. Tuck. 2008. *Caenorhabditis elegans* num-1 negatively regulates endocytic recycling. *Genetics*. 179:375–387. http://dx.doi.org/10.1534/genetics.108.087247

Nishimura, T., and K. Kaibuchi. 2007. Numb controls integrin endocytosis for directional cell migration with aPKC and PAR-3. *Dev. Cell*. 13:15–28. http://dx.doi.org/10.1016/j.devcel.2007.05.003

O'Connor-Giles, K.M., and J.B. Skeath. 2003. Numb inhibits membrane localization of Sanpodo, a four-pass transmembrane protein, to promote asymmetric divisions in *Drosophila*. *Dev. Cell*. 5:231–243. http://dx.doi.org/10.1016/S1534-5807(03)00226-0

Ohkuma, S., and B. Poole. 1978. Fluorescence probe measurement of the intralysosomal pH in living cells and the perturbation of pH by various agents. *Proc. Natl. Acad. Sci. USA*. 75:3327–3331. http://dx.doi.org/10.1073/pnas.75.7.3327

Pavlopoulos, E., C. Pitsouli, K.M. Klueg, M.A. Muskavitch, N.K. Moschonas, and C. Delidakis. 2001. *neuralized* encodes a peripheral membrane protein involved in delta signaling and endocytosis. *Dev. Cell*. 1:807–816. http://dx.doi.org/10.1016/S1534-5807(01)00093-4

Polo, S., and P.P. Di Fiore. 2006. Endocytosis conducts the cell signaling orchestra. *Cell*. 124:897–900. http://dx.doi.org/10.1016/j.cell.2006.02.025

Rhyu, M.S., L.Y. Jan, and Y.N. Jan. 1994. Asymmetric distribution of numb protein during division of the sensory organ precursor cell confers distinct fates to daughter cells. *Cell*. 76:477–491. http://dx.doi.org/10.1016/0092-8674(94)90112-0

Santolini, E., C. Puri, A.E. Salcini, M.C. Gagliani, P.G. Pelicci, C. Tacchetti, and P.P. Di Fiore. 2000. Numb is an endocytic protein. *J. Cell Biol.* 151:1345–1352. http://dx.doi.org/10.1083/jcb.151.6.1345

Sato, K., T. Watanabe, S. Wang, M. Kakeno, K. Matsuzawa, T. Matsui, K. Yokoi, K. Murase, I. Sugiyama, M. Ozawa, and K. Kaibuchi. 2011. Numb controls E-cadherin endocytosis through p120 catenin with aPKC. *Mol. Biol. Cell*. 22:3103–3119. http://dx.doi.org/10.1091/mbc.E11-03-0274

Seto, E.S., H.J. Bellen, and T.E. Lloyd. 2002. When cell biology meets development: endocytic regulation of signaling pathways. *Genes Dev.* 16:1314–1336. http://dx.doi.org/10.1101/gad.989602

Shaner, N.C., P.A. Steinbach, and R.Y. Tsien. 2005. A guide to choosing fluorescent proteins. *Nat. Methods*. 2:905–909. http://dx.doi.org/10.1038/nmeth819

Shcherbakova, D.M., and V.V. Verkhusha. 2013. Near-infrared fluorescent proteins for multicolor in vivo imaging. *Nat. Methods*. 10:751–754. http://dx.doi.org/10.1038/nmeth.2521

Smith, C.A., S.E. Dho, J. Donaldson, U. Tepass, and C.J. McGlade. 2004. The cell fate determinant numb interacts with EHD/Rme-1 family proteins and has a role in endocytic recycling. *Mol. Biol. Cell*. 15:3698–3708. http://dx.doi.org/10.1091/mbc.E04-01-0026

Song, Y., and B. Lu. 2012. Interaction of Notch signaling modulator Numb with α-Adaptin regulates endocytosis of Notch pathway components and cell fate determination of neural stem cells. *J. Biol. Chem.* 287:17716–17728. http://dx.doi.org/10.1074/jbc.M112.360719

Subach, F.V., G.H. Patterson, S. Manley, J.M. Gillette, J. Lippincott-Schwartz, and V.V. Verkhusha. 2009. Photoactivatable mCherry for high-resolution two-color fluorescence microscopy. *Nat. Methods*. 6:153–159. http://dx.doi.org/10.1038/nmeth.1298

Taylor, M.J., D. Perrais, and C.J. Merrifield. 2011. A high precision survey of the molecular dynamics of mammalian clathrin-mediated endocytosis. *PLoS Biol.* 9:e1000604. http://dx.doi.org/10.1371/journal.pbio.1000604

Tong, X., D. Zitserman, I. Serebriiskii, M. Andrake, R. Dunbrack, and F. Roegiers. 2010. Numb independently antagonizes Sanpodo membrane targeting and Notch signaling in *Drosophila* sensory organ precursor cells. *Mol. Biol. Cell*. 21:802–810. http://dx.doi.org/10.1091/mbc.E09-09-0831

Troost, T., S. Jaeckel, N. Ohlenhard, and T. Klein. 2012. The tumour suppressor Lethal (2) giant discs is required for the function of the ESCRT-III component Shrub/CHMP4. *J. Cell Sci.* 125:763–776. http://dx.doi.org/10.1242/jcs.097261

Uemura, T., S. Shepherd, L. Ackerman, L.Y. Jan, and Y.N. Jan. 1989. numb, a gene required in determination of cell fate during sensory organ formation in *Drosophila* embryos. *Cell*. 58:349–360. http://dx.doi.org/10.1016/0092-8674(89)90849-0

Upadhyay, A., V. Kandachar, D. Zitserman, X. Tong, and F. Roegiers. 2013. Sanpodo controls sensory organ precursor fate by directing Notch trafficking and binding γ-secretase. *J. Cell Biol.* 201:439–448. http://dx.doi.org/10.1083/jcb.201209023

Vaccari, T., and D. Bilder. 2005. The *Drosophila* tumor suppressor vps25 prevents nonautonomous overproliferation by regulating notch trafficking. *Dev. Cell*. 9:687–698. http://dx.doi.org/10.1016/j.devcel.2005.09.019

Venken, K.J., Y. He, R.A. Hoskins, and H.J. Bellen. 2006. P[acman]: a BAC transgenic platform for targeted insertion of large DNA fragments in *D. melanogaster*. *Science*. 314:1747–1751. http://dx.doi.org/10.1126/science.1134426

Verkhusha, V.V., N.A. Akovbian, E.N. Efremenko, S.D. Varfolomeyev, and P.V. Vrzheshch. 2001. Kinetic analysis of maturation and denaturation of DsRed, a coral-derived red fluorescent protein. *Biochemistry Mosc.* 66:1342–1351. http://dx.doi.org/10.1023/A:1013325627378

Yamashiro, D.J., and F.R. Maxfield. 1987. Acidification of morphologically distinct endosomes in mutant and wild-type Chinese hamster ovary cells. *J. Cell Biol.* 105:2723–2733. http://dx.doi.org/10.1083/jcb.105.6.2723

Yan, Y., N. Denef, and T. Schüpbach. 2009. The vacuolar proton pump, V-ATPase, is required for notch signaling and endosomal trafficking in *Drosophila*. *Dev. Cell*. 17:387–402. http://dx.doi.org/10.1016/j.devcel.2009.07.001

Yousefian, J., T. Troost, F. Grawe, T. Sasamura, M. Fortini, and T. Klein. 2013. Dmon1 controls recruitment of Rab7 to maturing endosomes in *Drosophila*. *J. Cell Sci.* 126:1583–1594. http://dx.doi.org/10.1242/jcs.114934

Zeng, C., S. Younger-Shepherd, L.Y. Jan, and Y.N. Jan. 1998. Delta and Serrate are redundant Notch ligands required for asymmetric cell divisions within the *Drosophila* sensory organ lineage. *Genes Dev.* 12:1086–1091. http://dx.doi.org/10.1101/gad.12.8.1086